PHYSICAL REVIEW A **88**, 062706 (2013)

Major role of multielectronic K-L intershell resonant recombination processes in Li- to O-like ions of Ar, Fe, and Kr

C. Beilmann,[1] Z. Harman,[1,2] P. H. Mokler,[1] S. Bernitt,[1] C. H. Keitel,[1] J. Ullrich,[1] and J. R. Crespo López-Urrutia[1]

[1]*Max-Planck-Institut für Kernphysik, Saupfercheckweg 1, 69117 Heidelberg, Germany*

[2]*ExtreMe Matter Institute (EMMI), Planckstraße 1, 64291 Darmstadt, Germany*

(Received 27 May 2013; published 10 December 2013)

Dielectronic and higher-order resonant electron recombination processes including a K-shell excitation were systematically measured at high electron energy resolution in electron beam ion traps. After storing highly charged Ar, Fe, and Kr ions, the dependence on atomic number Z of the contribution of these processes to the total recombination cross section was studied and compared with theoretical calculations. Large higher-order resonant recombination contributions were found, especially for systems with $10 < Z < 36$. In some cases, they even surpass the strength of the dielectronic channel, which was hitherto presumed to be always the dominant one. These findings have consequences for modeling high-temperature plasmas. Features attributed to intershell quadruelectronic recombination were also observed. The experimental data obtained for the He-like to O-like isoelectronic sequences compare well with the results of advanced relativistic distorted-wave calculations employing multiconfiguration Dirac-Fock bound-state wave functions that include threefold and fourfold excitations.

DOI: 10.1103/PhysRevA.88.062706 PACS number(s): 34.80.Lx, 32.80.Hd, 52.25.Os

I. INTRODUCTION

Electron-electron interaction is a fundamental aspect of both atomic and molecular structure and reactions. It governs the level structure and the time dependence of atomic collision processes and thus also the behavior of laboratory and astrophysical plasmas. Understanding electronic correlations and their consequences is therefore of great importance for the development of theory, and a good knowledge of those is crucial for all aspects of plasma diagnostics.

Among the different processes involving electron-electron interaction, dielectronic recombination (DR) and its time reversal, the Auger decay following photoexcitation of inner-shell electrons [1,2], are preeminent. In the first-order DR process [see left panel in Fig. 1(a)], a free electron is captured in a collision with an ion, thereby transferring energy to another bound electron and exciting it resonantly. The ion is then left in a (usually) doubly-excited state which can decay radiatively, completing the DR process. Extended experimental and theoretical investigations on DR with highly charged ions (HCI) have been carried out in recent years by various groups (e.g., [3–11]).

Usually, DR is described in an independent-particle model, only taking into account the interaction between the two electrons involved: the initially free one and an active bound one. Higher-order electron correlations are not accounted for in this approach. This is illustrated in Fig. 1(b) (left panel), where the interaction process is represented by the Feynman diagram of one virtual photon exchange. Hence, the DR process is usually denoted by the states of the electrons of concern; for instance, a K-LL DR process (Auger notation, cf. [12]) denotes the excitation of an inner-shell K electron to the L shell with a resonant capture of the free electron also to the L shell. However, our recent investigations have shown that higher-order correlations with the active excitation of more than one electron may contribute considerably to recombination and may affect plasma parameters noticeably [13,14]. We focus on these higher-order effects in this paper.

Trielectronic recombination (TR) as an *intrashell* process, where two bound L-shell electrons are excited within their shell through the capture of one free electron, was reported as a result of low-energy storage-ring DR measurements (cf. [15–17]). In our previous experiments with electron beam ion traps (EBIT), we found that the higher-order recombination process can also lead to far more energetic *intershell* excitations [13,14] with a rather large contribution. The corresponding process with $\Delta n = 1$ excitation is exemplified in the middle diagram in Fig. 1 showing an intershell KL-LLL TR process, where a K-shell electron and an L-shell electron are excited simultaneously to vacant higher-lying L levels under resonant capture of the free electron, here also to the L shell.

As more than two electrons are actively involved in TR, independent-particle models such as the (Dirac-)Hartree-Fock method cannot adequately describe it. Electron correlations must be included using, e.g., multiconfiguration or many-body perturbation theory methods. Within the perturbative picture (at least) two virtual photons must be exchanged for TR. Three out of six possible interactions are shown in the middle panel of Fig. 1(b).

Intershell TR in highly ionized Kr ions was observed and compared [13] with extended calculations based on the multiconfiguration Dirac-Fock (MCDF) procedure [8,13,18]. In that work, the first indications of third-order intershell quadruelectronic recombination (QR) were also found. On the right side of Fig. 1, intershell KLL-$LLLL$ QR is visualized. Here, electron capture to the L shell occurs simultaneously with the excitation of a K-shell electron, while two further L-shell electrons are also resonantly excited to higher-lying L states. Feynman diagrams with three exchanged virtual photons are shown in Fig. 1(b) (3 out of 24 possibilities are depicted).

In our more recent work [14], higher-order intershell recombination effects have also been reported for highly charged Ar and Fe ions. We found that TR could overwhelm the first-order DR process for some ionic species in light elements, being the dominant recombination channel in those systems.

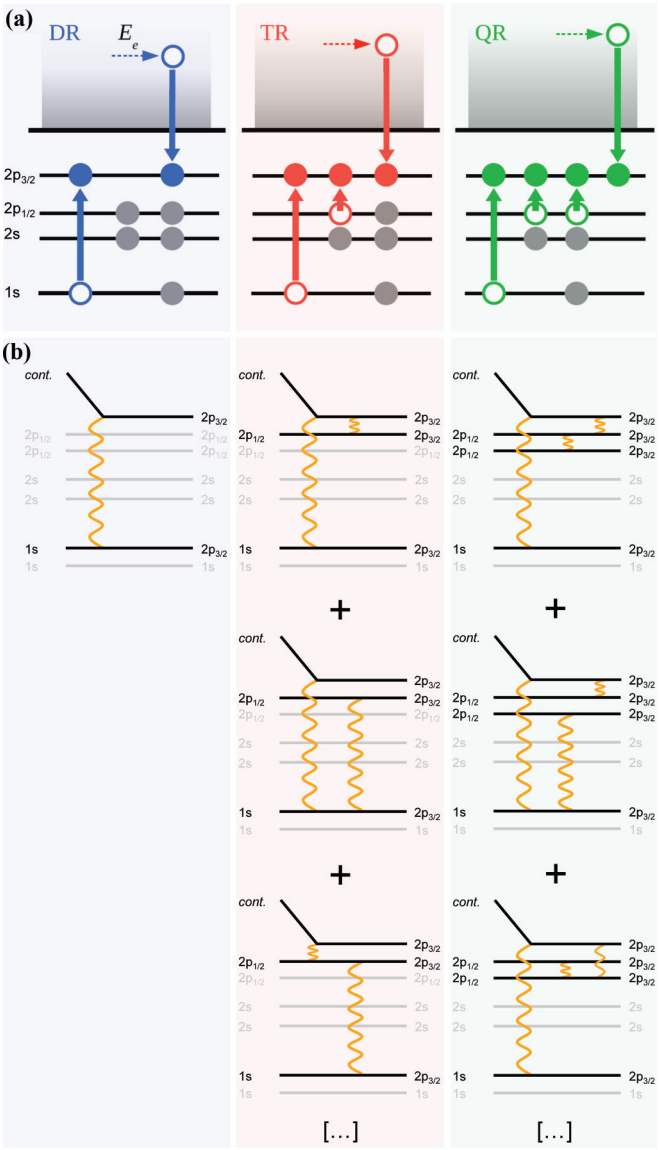

FIG. 1. (Color online) Schematic diagrams for first- and higher-order resonant electronic recombination (C-like ions): dielectronic recombination [DR, left panel in blue (dark gray)], trielectronic recombination [TR, middle panel in red (medium gray)], and quadruelectronic recombination [QR, right panel in green (light gray)]. (a) Energy-level diagrams are shown. (b) The Feynman diagrams show some interaction possibilities.

In this paper we report in detail on our systematic high-resolution resonant recombination measurements performed at two of the EBITs at the Max-Planck-Institut für Kernphysik in Heidelberg, Germany, namely, the HD-EBIT [19] and FLASH-EBIT [20]. We have extended the range of observed isoelectronic sequences, ranging now from He-like to O-like ions.

For the observation of the weak and blended higher-order structures, high-resolution experimental techniques are required. Therefore, we give also insight into the forced evaporative ion cooling technique, essential for high-resolution experiments. With this method, lower-Z elements, which require higher absolute resolution because of their lower fine-structure splittings, become more readily accessible. This is mandatory for the aim of our investigations because in the low-Z regime, electron correlations are expected to become stronger due to the relative decrease of the central Coulomb force compared to the Z-independent electron-electron interaction.

Our studies cover a range of elements relevant to different fields of plasma physics: the study of Fe ions is central in astrophysics, and Ar as well as Kr ions have diagnostic uses, e.g., in fusion plasma devices [21–23].

II. THEORETICAL APPROACH

In a resonant recombination process, resonant electron capture is followed by the radiative decay and stabilization of the ion's intermediate autoionizing state. It proceeds from an initial state i, consisting of the ground-state ion and a continuum electron with an asymptotic momentum $\vec{p}$, through the intermediate autoionizing state d to the bound final state f. The cross section for a specific resonant recombination channel is given (in atomic units) as a function of the electron's kinetic energy E in terms of the resonance strengths $S_{i\to d\to f}$ as (see, e.g., [24–26])

$$\sigma_{i\to d\to f}(E) = S_{i\to d\to f} L_d(E)\,,$$
$$S_{i\to d\to f} = \frac{2\pi^2}{p^2}\frac{2J_d+1}{2(2J_i+1)}\frac{\Gamma^r_{d\to f}}{\Gamma_d}\Gamma^a_{d\to i}\,. \qquad (1)$$

Here, the Lorentzian line-shape function

$$L_d(E) = \frac{\Gamma_d/(2\pi)}{(E-E_{\rm res})^2+\Gamma_d^2/4} \qquad (2)$$

is normalized to unity on the energy scale, $\int L(E)dE = 1$, and is centered around the resonance energy $E_{\rm res}$, calculated as the difference of the intermediate and initial ionic level energies: $E_{\rm res} = E_d - E_i$. J_d and J_i are the total angular momenta of the intermediate and the initial states of the recombination process, respectively. The free-electron momentum associated with the kinetic energy of the initially free electron at resonance is given by $p = |\vec{p}| = \sqrt{(E_{\rm res}/c)^2 - c^2}$. The total radiative width of the autoionizing intermediate state is $\Gamma^r_d = \sum_f \Gamma^r_{d\to f}$, and $\Gamma^a_d = \sum_i \Gamma^a_{d\to i}$ is the total autoionization width of the same state, summed over all possible Auger final states. Γ_d denotes the total natural linewidth of the resonant state: $\Gamma_d = \Gamma^r_d + \Gamma^a_d$. The resonant capture rate is related to the rate of its time-reversed (Auger) process by the principle of detailed balance and is defined, according to Fermi's golden rule, perturbatively as

$$\Gamma^{\rm capt}_{i\to d} = \frac{2J_d+1}{2(2J_i+1)}\Gamma^a_{d\to i} = \frac{2\pi}{2(2J_i+1)}\sum_{M_d}\sum_{M_i m_s}\int \sin(\theta)d\theta d\varphi |\langle \Psi_d; J_d M_d \Pi_d | V | \Psi_i E; J_i M_i \Pi_i, \vec{p} m_s\rangle|^2$$
$$= 2\pi \sum_\kappa |\langle \Psi_d; J_d \Pi_d || V || \Psi_i E; J_i \Pi_i j\pi; J_d \Pi_d\rangle|^2\,. \qquad (3)$$

In this equation, the transition amplitude, i.e., the matrix element of the sum of the Coulomb and Breit interactions $V = V^C + V^B$, is calculated with the initial bound-free antisymmetrized product state $|\Psi_i E; J_i M_i \Pi_i, \vec{p} m_s\rangle$ and the resonant intermediate state. After averaging over the initial magnetic quantum numbers M_i, m_s and the direction (θ,ϕ) of the incoming continuum electron and after performing a summation over the magnetic quantum numbers M_d of the autoionizing state, one obtains the partial-wave expansion of the reduced matrix elements, as given in the last line of Eq. (3). κ is the relativistic angular momentum quantum number appearing in the decomposition of the continuum scattering state [27]. The last line of Eq. (3) also shows that, owing to the usual Coulomb interaction (or, generally, electron-electron interaction) selection rules, the total angular momentum of the initial state (consisting of the bound ionic electrons and the continuum electron partial wave) and that of the autoionizing state must be equal. The same holds for the parities Π (given as the product of the single-electron parities) of the initial and autoionizing states.

In the case of dielectronic recombination, the autoionizing state may be approximately described by a single configuration state function. For example, for C-like ions initially in their ground sate, $|\Psi_i\rangle = |1s^2 2s^2 2p_{1/2}^2\rangle$, the K-LL DR autoionizing states may be $|1s2s^2 2p_{1/2}^2 2p_{3/2}^2, J_d \Pi_d\rangle$, with $J_d = \{1/2,3/2,5/2\}$ and $\Pi_d = +1$. This notation expresses that a configuration state function is constructed from antisymmetrized single-particle wave functions coupled to a given J_d. Such states and the corresponding energy levels may be calculated by the multiconfiguration Dirac-Hartree-Fock (MCDF) approach with additional quantum electrodynamic and mass shift corrections [8,28,29]. The bound-state wave functions obtained numerically may be used to construct continuum orbitals and the matrix elements entering Eq. (3) [8,25,26,30].

The transition amplitude of the three-body interaction accounting for trielectronic recombination into a state $|1s2s^2 2p_{1/2} 2p_{3/2}^3, J_d \Pi_d\rangle$ may be described in a perturbative approximation as

$$\frac{\langle 1s2s^2 2p_{1/2} 2p_{3/2}^3, J_d \Pi_d | V | 1s2s^2 2p_{1/2}^2 2p_{3/2}^2, J_d \Pi_d \rangle}{E_{'\mathrm{TR}'} - E_{'\mathrm{DR}'}} \times \langle 1s2s^2 2p_{1/2}^2 2p_{3/2}^2, J_d \Pi_d | V | 1s^2 2s^2 2p_{1/2}^2 E; J_i j; J_d \Pi_d \rangle. \quad (4)$$

Here, $E_{'\mathrm{TR}'}$ and $E_{'\mathrm{DR}'}$ stand for the energy eigenvalues associated with states $|1s2s^2 2p_{1/2} 2p_{3/2}^3, J_d \Pi_d\rangle$ and $|1s2s^2 2p_{1/2}^2 2p_{3/2}^2, J_d \Pi_d\rangle$, respectively. Note that since the operator V is a two-body operator, i.e., it only changes the occupation numbers of two single-electron states, the trielectronic process cannot be described by first-order perturbation theory,

$$\langle 1s2s^2 2p_{1/2} 2p_{3/2}^3, J_d \Pi_d | V | 1s^2 2s^2 2p_{1/2}^2 E; J_i \Pi_i j\pi; \times J_d \Pi_d \rangle = 0\,. \quad (5)$$

Equation (4) also expresses the symmetry requirement that a TR autoionizing state can only be populated with noticeable probability if there is a DR state of the same total angular momentum and parity (i.e., the matrix element in the numerator is nonzero) and it is close in energy (i.e., the denominator is not too large compared to the numerator). This acts toward a suppression of KL-LLL-TR for initially Be-like ions [13]: starting with the Be-like initial state, characterized by the dominant configuration $1s^2 2s^2$, KL-LLL TR may only populate two-hole autoionizing states such as $1s2s2p^3$, which are of negative parity. The nearby K-LL DR single-hole autoionizing states are of the type $1s2s^2 2p^2$ and of positive parity; therefore, these DR and TR autoionizing states do not mix [i.e., the ratio in the first line of Eq. (4) is zero because of the Coulomb interaction selection rules]. Higher-lying DR states, i.e., those of type $1s2s^2 2p3s$, may certainly possess negative parity and mix with the TR state; however, as such states are energetically far away from the TR state, the mixing is low [i.e., the energy denominator in the first line of Eq. (4) is large].

The TR cross section may nevertheless be sizable due to the mixing of the initial (ground) state of the ion with excited-state configurations: since in the description of the, e.g., Be-like initial state configurations of the type $1s^2 2p^2$ are present, the transition from such a state to a TR configuration $1s2s2p^3$ is possible by a single Coulomb interaction, giving rise to significant TR peaks [31]. This demonstrates that for an adequate description of resonant recombination processes, mixing effects in both the initial and intermediate states have to be taken into account.

The ratio of TR to DR amplitudes is given by the fraction in the first line of Eq. (4). At low Z, this fraction may approach unity since the electron interaction operator V acts on the strongly overlapping TR and DR state functions, and the interaction energy in the numerator lies close to the $(E_{'\mathrm{TR}'} - E_{'\mathrm{DR}'})$ splitting. The TR capture rates may thus become comparable to the DR capture rates. Because of this, it is necessary to treat the trielectronic process nonperturbatively: the autoionizing state formed by the trielectronic process is described as the linear combination

$$|\mathrm{TR}\rangle = c_1 |1s2s^2 2p_{1/2} 2p_{3/2}^3, J_d \Pi_d\rangle + c_2 |1s2s^2 2p_{1/2}^2 2p_{3/2}^2, J_d \Pi_d\rangle, \quad (6)$$

and the autoionizing state populated by dielectronic capture is represented as

$$|\mathrm{DR}\rangle = \tilde{c}_1 |1s2s^2 2p_{1/2}^2 2p_{3/2}^2, J_d \Pi_d\rangle + \tilde{c}_2 |1s2s^2 2p_{1/2} 2p_{3/2}^3, J_d \Pi_d\rangle. \quad (7)$$

The expansion coefficients may be obtained by diagonalizing the total Hamiltonian of the system in a configuration interaction approach or by the MCDF method.

Note that in Eqs. (6) and (7), the first configuration is not necessarily the dominant one; this holds true in only the high-Z limit where the jj-coupling scheme is applicable. The question may arise whether it is meaningful to define the number of electrons excited in a correlated many-electron shell, which may be described by strongly mixing configurations in the low-Z limit. We find that, since a state such as (6) contains two electronic holes, one in the K shell and one in the L shell, which may both decay separately by photon emission, the process leading to its population can indeed be termed trielectronic recombination.

Equations (6) and (7) may be easily extended to the case when three or more levels sharing the same $J_d \Pi_d$ quantum numbers are energetically close. Correlation effects may be accounted for more accurately by including further configurations of the same symmetry $J_d \Pi_d$ in a multiconfiguration approach.

III. EXPERIMENTAL PROCEDURE

Resonant recombination was experimentally investigated by using electrons as projectiles and HCI as targets. The target ions are produced and confined in an EBIT by electron impact ionization of neutral target atoms. Electron beams with currents of 50 to 200 mA compressed to typical diameters of around 50 μm by a magnetic field of 6 to 8 T ensured a high current density in the reaction volume and thus a high ionization rate. This current density leads to a negative space-charge potential that confines the positively charged ions in the radial direction around the electron-beam axis. An arrangement of drift tubes allows for generating a potential well to trap the ions in the axial direction. This basic principle of an EBIT is displayed in Fig. 2.

Projectile electrons are provided by the monoenergetic electron beam of the EBIT. Its energy is controlled by the voltage difference between the cathode of the electron gun (V_{cath}) and the central drift tube surrounding the reaction volume ($V_{\text{DT 2}}$). The variable bias acceleration voltage $V_{\text{DT pot}}$ is applied to all drift tubes, while keeping the ions trapped within a potential well of constant depth determined by the potential difference between the central drift tube and its immediate neighboring electrodes. We have used the FLASH EBIT [20] for the Ar and Fe experiments and the Heidelberg EBIT [19] for the Kr measurements. The experimental procedure was the same in both devices.

For the experiments, we follow the widely applied scheme described in Ref. [32]. Here, we slowly vary the electron-beam energy across a range of interest in a sawtooth ramp with a slow slew rate of 2 V/s in order to ensure steady-state conditions. Recombination involving K-L excitation was monitored by measuring the characteristic K x-ray photons that are emitted by radiative stabilization of the K-hole excited state formed by resonant electron capture. At specific electron energies, an enhancement of K-photon emission indicates a photorecombination resonance. A high-purity germanium x-ray detector is pointed at the reaction volume side-on with respect to the electron beam through a 250-μm-thick beryllium window. For the photon energy range of interest (from 2 to 14 keV) this window is nearly transparent.

Given the very high electron impact ionization rates of the low-charge states (L-shell ions from fluorinelike to berylliumlike), the ion charge distribution in those states is not strongly affected by the strong recombination resonances. Therefore, we can assume for simplicity that the ratio of recombination strengths for resonances belonging to the same charge states are approximately equal to the observed intensity ratios. However, for the lithiumlike electron impact ionization the rates are lower since only one electron is left in the L shell. This leads to a depletion of the population of heliumlike ions at strong DR resonances, which has to be taken into account for absolute comparisons.

A two-dimensional intensity plot depending on the electron-beam energy and the emitted x-ray photon energy is displayed in Fig. 3 (top panel). The electron recombination resonances appear as bright spots. In Fig. 3 (top), an overview of resonant recombination processes with K-shell excitation in He- to O-like Ar is presented, showing both the K-LL region this paper is focused on and resonances for K-LM, K-LN, etc., recombination processes. These resonances involving the K shell and a higher shell can also be seen as bright spots in the K_β photon energy region. In addition, K-MM resonances can be identified at electron-beam energies around 3.25 keV. The projections shown in Fig. 3 (bottom panel) represent the K_α emission (K_α cut) and K_β and higher emission as a function of the electron energy.

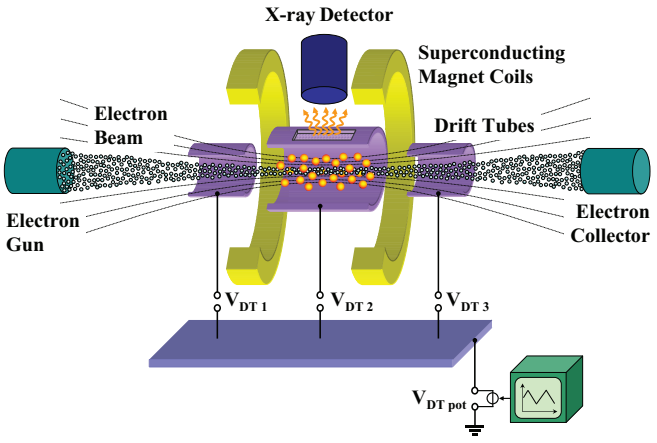

FIG. 2. (Color online) Principle of electron recombination experiments using an electron beam ion trap. The whole drift tube assembly (including the central tube, V_{DT2}) can be ramped by the common platform V_{DTpot}. Photons resulting from radiative stabilization are detected with an energy-dispersive germanium detector.

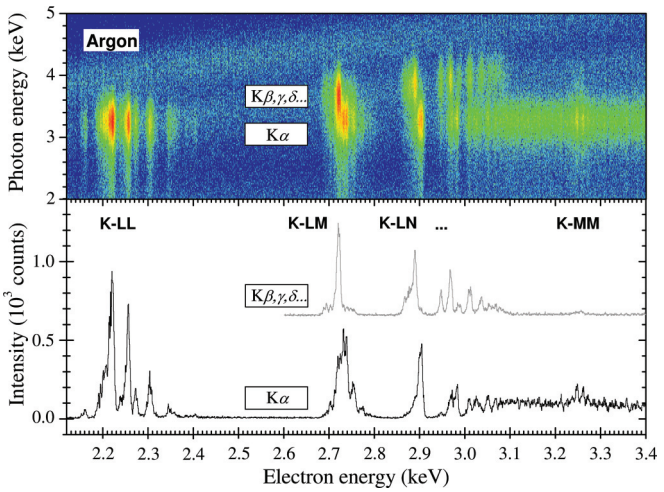

FIG. 3. (Color online) (top) Photon intensity map (vertical: photon energy; horizontal: electron energy) showing an overview of the photorecombination process for trapped Ar ions with an open L shell. The bright features correspond to resonances. (bottom) Projections onto the electron energy axis of stripes containing the K_α and K_β emission lines (lower and upper spectra, respectively).

For the investigation of weak resonances, a good resolution on the electron energy is a prerequisite for separating them from stronger lines. In an EBIT, the resolution in recombination measurements is limited by the energetically broadened electron beam [33,34]. Earlier experiments used low electron-beam currents for minimizing the absolute space-charge potential, its width, and the ion heating caused by electron impact [34]. However, a low beam current leads to a strong reduction of the ion production rate and also to a diminished recombination rate.

In our experiments we improved the resolution by forced evaporative cooling in combination with electron-beam currents sufficient for an efficient ionization and abundant recombination yield. This was realized by lowering the axial potential well applied to the drift tubes. To compensate a remaining trap generated by the space-charge potential of the drift tubes with different diameters [34,35], a positive offset voltage has to be applied to the central drift tube relative to the surrounding ones. Under these settings, only a cold ion ensemble remains in the trap, and the measurements can be performed with relatively high electron-beam currents.

With this method, the resolution, defined as the ratio of the FWHM width to the space charge, was improved by roughly a factor of 5 in comparison with the common measurement scheme [35]. Figure 4(a) demonstrates this advantage for two strong adjacent DR resonances in C-like Kr ions, namely, the $([1s2s^2 2p_{1/2}^2(2p_{3/2}^2)_2]_{5/2,(3/2+1/2)})$ lines. The resolution (FWHM) of the resonance with $J = 5/2$ is plotted versus the voltage of the central drift tube with respect to the outer ones at an electron-beam current of 200 mA. The former unresolved lines become clearly separated at the optimized point of cooling. In Fig. 4(b), a very well resolved recombination spectrum allows for both a clear separation of charge-state-specific resonances and the observation of otherwise blended weak features.

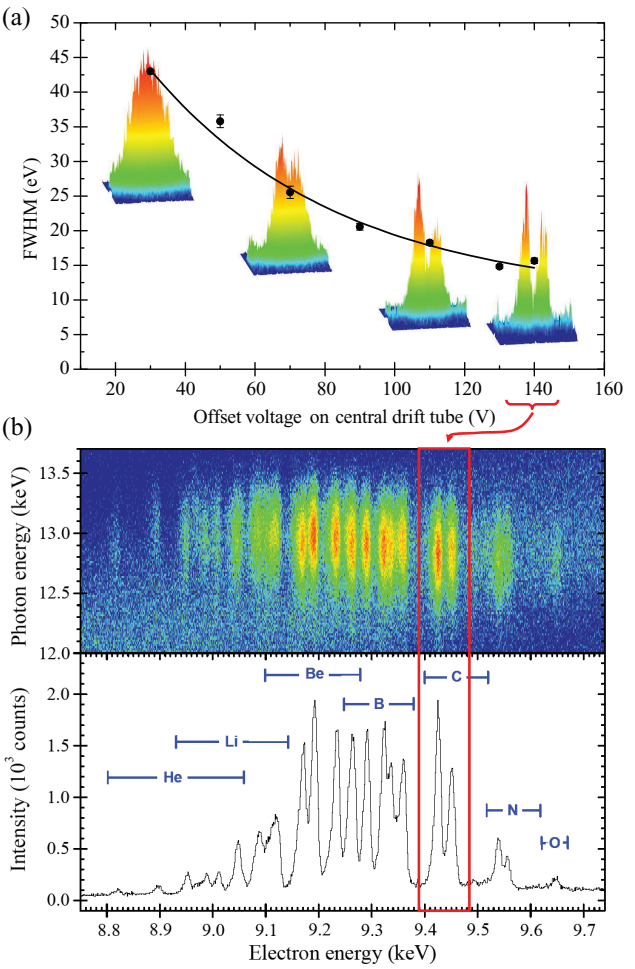

FIG. 4. (Color online) (a) Resolution improvement by evaporative cooling: Measured resolution (FWHM) for DR resonances in C-like Kr (around 9.44 keV) plotted as a function of the offset voltage ΔV_{DT2} of the central drift tube. The inserted diagrams give the three-dimensional intensity plots at offset voltages of 30, 60, 110 and 140 V. (b) Resulting photorecombination spectrum for He- to O-like Kr ions. The region of interest for C-like ions displayed in (a) is indicated; the regions for the different ionic sequences are labeled.

IV. RESULTS AND DISCUSSION

We investigate the K-LL energy region of resonant recombination into the He- to O-like charge states of Ar, Fe, and Kr ions in order to gain insight into the Z behavior of resonance energies and strengths and the systematics of higher-order processes. In an EBIT, different charge states of an element are stored simultaneously. By using a constant strong injection of neutrals, the charge-state distribution can be made sufficiently flat in order to make recombination resonances from He- to O-like ions appear together in the spectra. The high resolution allows for a good separation of the resonance groups for different ionic species, as indicated in Fig. 5 by bars above each spectrum.

In Fig. 5, we show the recombination spectra of the investigated ions in the specified energy region. We calibrate the electron energy scale by taking the predicted values of two well-separated resonance lines of He-like ions which have small theoretical uncertainties. In the case of Ar it was possible to use two strong resonances from the K-LL and K-LM regions. In order to account for the Z dependence of the resonance energies, the energy scales of the spectra are normalized by multiplying by a factor $1/Z^2$ (Rydberg scaling).

The curves shown in Fig. 5 display resonance energies and relative resonance strengths, as well as the respective Z dependences. In the normalized representation given, the Z dependences of the resonance energies (beyond the dominant Z^2 dependence) can be seen.

In Fig. 6, we compare our recombination spectra for the astrophysically relevant Fe ions with our theoretical predictions, where the abundances of the different charge-state fractions have been adjusted to match the measured ones.

In general, a very good agreement both in the position of the resonances relative to those of the calibration resonances of He-like ions and in (relative) resonance strengths can be stated. This strengthens our confidence in the reliability of the calculations also for higher-order resonances, which we identify based on their predicted energy values.

Contributions from TR resonances can clearly be seen in Fig. 6 (as well as in Fig. 5) for initially B-like, C-like, and N-like ions around 4.88, 4.95, and 5.04 keV, respectively. The

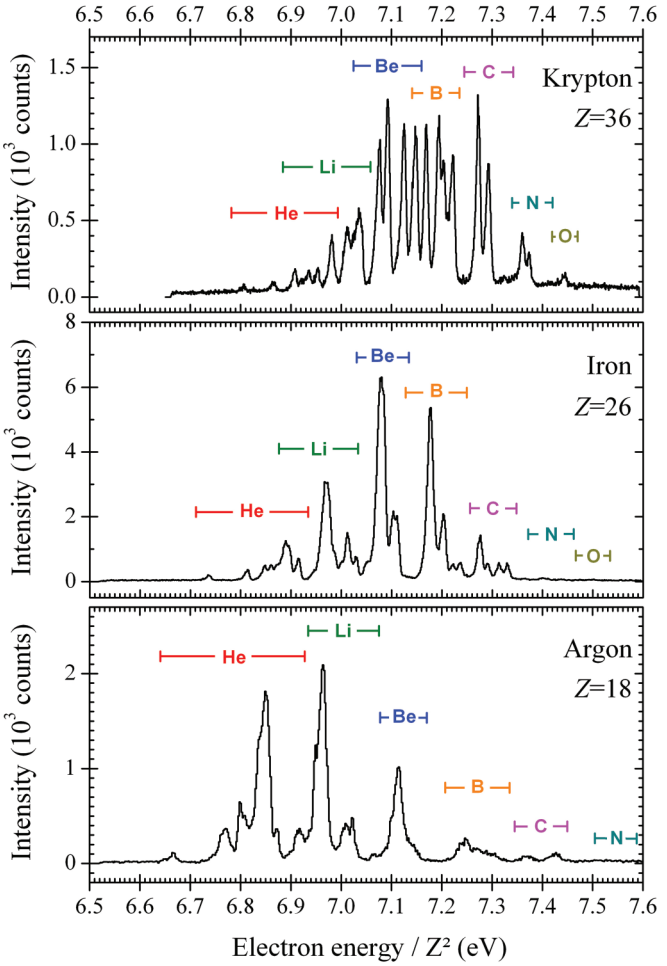

FIG. 5. (Color online) Electronic recombination spectra in the energy region of the K-LL DR resonances and their higher orders (especially TR) in highly charged Kr, Fe, and Ar ions. The electron energy scales are multiplied by a factor $1/Z^2$.

DR spectrum for Li-like ions is especially rich and broad for K-L excitation since not only are the $2p$ levels accessible but also the $2s$ level has a vacancy. According to the calculations, TR resonances from Li-like ions are hidden under the strong DR lines of the Be-like sequence.

Beyond the lowest-order Z^2 scaling of the binding energy, we have to consider the electron-electron interaction decreasing with Z^{-1} in importance relative to the central Coulomb force and relativistic effects increasing rapidly with Z^4 for heavy ions. For the heavier species, the influence of the latter is dominant. The range of ions studied here is characterized by a transition from the electron correlation-dominated range to one dominated by relativistic effects, already leading here to a large fine-structure splitting. Hence, for the heavier system of Kr, and to some extent also for Fe, we find more lines resolved in the spectra. For the measurement with Ar ions, the resonances within one charge state overlap more strongly, and despite the high experimental absolute resolution of only about 5 eV, they can be barely resolved. In comparison to the transition energies, the relative resolution is roughly equivalent to the absolute one of 13 eV seen in the case of Kr as the heaviest considered element.

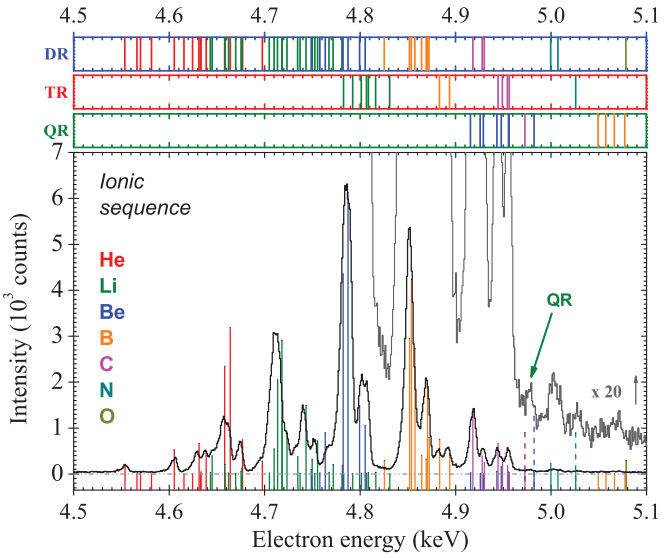

FIG. 6. (Color) Comparison of the Fe photorecombination spectrum with our theoretical predictions. To show weak details, a 20-fold magnified spectrum is also displayed. On the top, the resonances belonging to different recombination orders are indicated separately and are color-coded according to their He-like to O-like charge states.

In Fig. 7 we show the Z dependence of the relative resonance energies for the strongest recombination lines of initially He-like to O-like ions. The curves normalized by Z^2 are based on our theoretical values including electron-electron correlations. These spectra show clearly the transition region

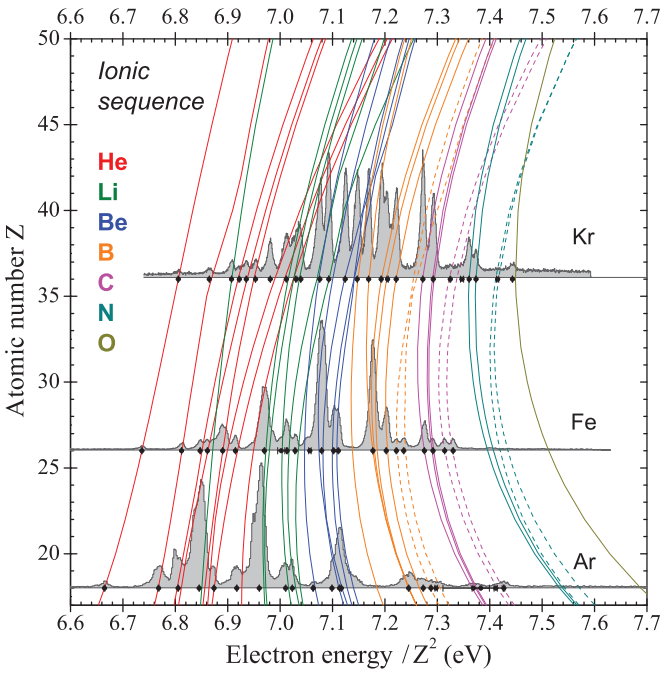

FIG. 7. (Color) Photorecombination resonance energies for ions as a function of the atomic number Z; the resonance energies are normalized by Z^2. The calculations are described in Sec. II. Experimental values from the measured spectra for $Z = 18$, 26, 36 (Ar, Fe, Kr, respectively) appear as dots overlaid in gray. Trielectronic recombination resonances are marked by dashed lines.

from the strong electron-electron interaction at low Z to the increased relativistic influence at higher Z. These trends are confirmed experimentally, as spectra for Ar, Fe, and Kr overlaid on the graph in Fig. 7 demonstrate.

We now discuss the resonance strengths of C-like ions, which, among all isoelectronic sequences with an open L shell, are expected to have the strongest TR contributions. The occupation rules, partially also in combination with parity rules (cf. Sec. II), allow for several resonances. With initially four vacancies in the open L shell and with two $2s$ as well as $2p$ electrons, many possible excitation as well as relaxation channels for TR processes appear. In contrast, the B-like sequence has a smaller number of excitable electrons, and N-like ions contain fewer vacancies in which excitation can occur. For the Li-like sequence there is only one $2s$ electron left for the additional intrashell excitation in TR. These differences in the recombination strengths of TR in different ionic sequences are illustrated below in Fig. 11.

The region of interest of the recombination spectra for the C-like isoelectronic sequence is enlarged in Fig. 8. The resonance areas for DR and TR are indicated in blue (dark gray) and red (medium gray), respectively. For Kr the spectrum is equivalent to our data from [13], with the two prominent DR double lines for C-like ions (at 7.27 and 7.28 eV/Z^2) followed by the double DR line for N-like Kr ions (at 7.36 and 7.37 eV/Z^2). In between (at around 7.32 eV/Z^2) we find the faint structure for the C-like TR process contributing in total only 6% to all the resonant recombination processes in this C-like case.

Proceeding down in Z to the Fe ions, the importance of electron-electron interaction increases, and correspondingly, TR can be expected to be more important there. For C-like Fe ions we find the K-LL DR double line at 7.28 and 7.30 eV/Z^2 and the KL-LLL TR double line at 7.32 and 7.34 eV/Z^2; however, the relative TR contribution increases already dramatically to about 50% of the DR contribution [14].

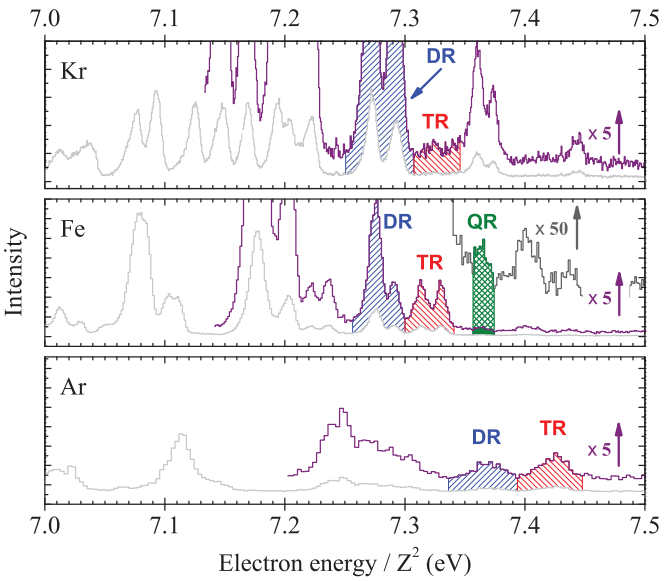

FIG. 8. (Color online) Partial magnified spectrum showing photorecombination resonances of Be-like to N-like ions of Ar, Fe, and Kr. DR, TR, and QR processes are marked for C-like ions.

Continuing further down in Z to Ar, the doublets for C-like ions are not any more resolved experimentally due to the reduced fine-structure splitting of the contributing different j components (see the broad K-LL DR line at 7.37 eV/Z^2). The stronger line around 7.42 eV/Z^2 corresponds to the higher-order KL-LLL TR process of C-like Ar ions. Here, the TR process overwhelms already the corresponding first-order K-LL DR by a factor of about 1.5. This strong effect shows how higher-order electron-electron correlation can surpass the (intuitively stronger) first-order process [14].

In order to understand this unexpected increase in the relative importance of the higher-order process of TR at low Z compared to DR, one has to consider the absolute resonance strength. Following the general formula (1), it can be described as the product of the Auger rate responsible for the population of the excited intermediate state and the fluorescence yield determining its decay to the final state. The fluorescence yield is determined by the ratio of the radiative decay rate to the total decay rate, which is the sum over all possible radiative and Auger channels.

The calculated Z scalings for the contributing parameters for selected DR and TR resonances in initially C-like ions are sketched in Figs. 9 and 10. Resonances with total angular momenta $J = 5/2$ and $J = 3/2$ have been selected for demonstration; note that DR and TR states may mix with each other within a set of levels possessing the same J. The radiative rates [Figs. 9(b) and 10(b)] increase generally with $\Gamma^r \propto Z^4$ (see, e.g., [2] or the overview in [36]), whereas the normal (two-electron) Auger rates [Figs. 9(c) and 10(c)], relevant for DR, are almost Z independent, $\Gamma^{a,2e} \propto Z^0$. Relativistic wave function and Breit interaction corrections introduce terms scaling with even powers of Z at higher charge numbers [37]; however, these are not of high relevance for the light and medium-heavy elements where higher-order recombination processes are observable.

For high Z values, in the case of DR, the fluorescence yield is dominated by the radiative decay, and thus it approaches unity, whereas for small Z it is governed by the Auger rate [see Fig. 9(d)]. Following Eq. (1) and including the phase-space factor $1/p^2 \approx 1/(2E)$, this yields the following scaling law for the strength [38,39]:

$$S^{\mathrm{DR}} \propto \frac{1}{Z^2}\frac{Z^4 Z^0}{a_1 Z^4 + a_2 Z^0} = \frac{1}{a_1 Z^2 + a_2 Z^{-2}}\,. \qquad (8)$$

Thus, in a simple nonrelativistic approximation, the DR strength is roughly proportional to Z^2 at low atomic numbers, decreases for high Z with $1/Z^2$, and is almost constant in the mid-Z region.

In a similar way, scaling laws may be derived for the higher-order resonances. The Z dependence of the contributing parameters for the TR processes are shown as dashed lines in Figs. 9 and 10. The Auger rates causing the higher-order resonances show a somewhat different behavior. The perturbative factor in the first line of Eq. (4) introduces an additional scaling factor of $1/Z$ to the transition amplitude of TR; therefore, the three-electron Auger rates (and the TR capture rates) decrease approximately as $\Gamma^{a,3e} \propto Z^{-2}$ at high Z values. This three-electron Auger rate has also to be taken into consideration in the calculation of the total decay rate, and thus, the Z scaling of the TR resonance strength follows the

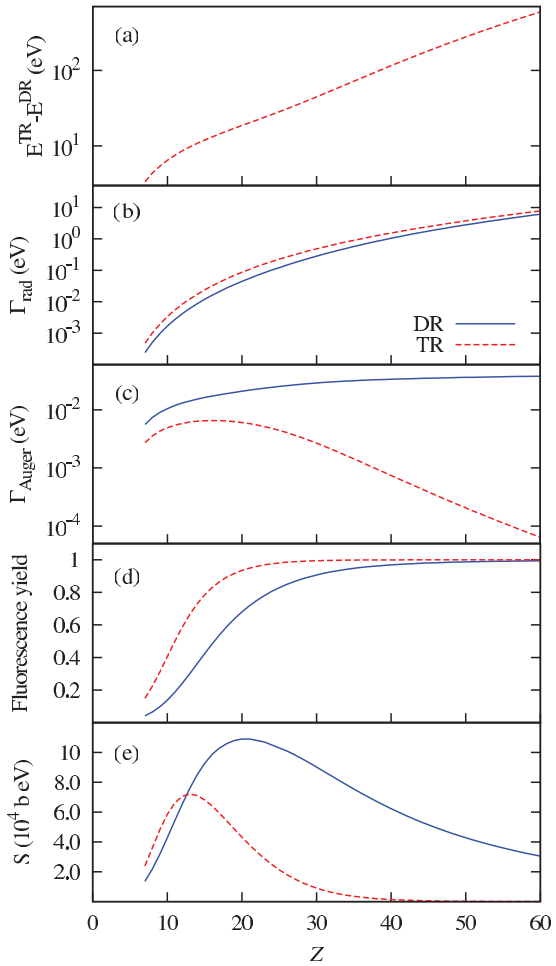

FIG. 9. (Color online) Theoretical scaling of different atomic quantities contributing to the DR and TR resonant recombination resonance strength as a function of Z for $J = 5/2$ resonances in initially C-like ions. (a) Difference of TR and DR resonance energies, (b) radiative decay rates, (c) Auger decay rates, (d) fluorescence yields, and (e) resonance strengths. The quantities are given for the case of the $1s2s^22p_{1/2}^2(2p_{3/2}^2)_2$ $J = 5/2$ DR resonance (solid blue line) and the $(1s2s^22p_{1/2})_1 2p_{3/2}^3$ $J = 5/2$ TR resonance (dashed red line).

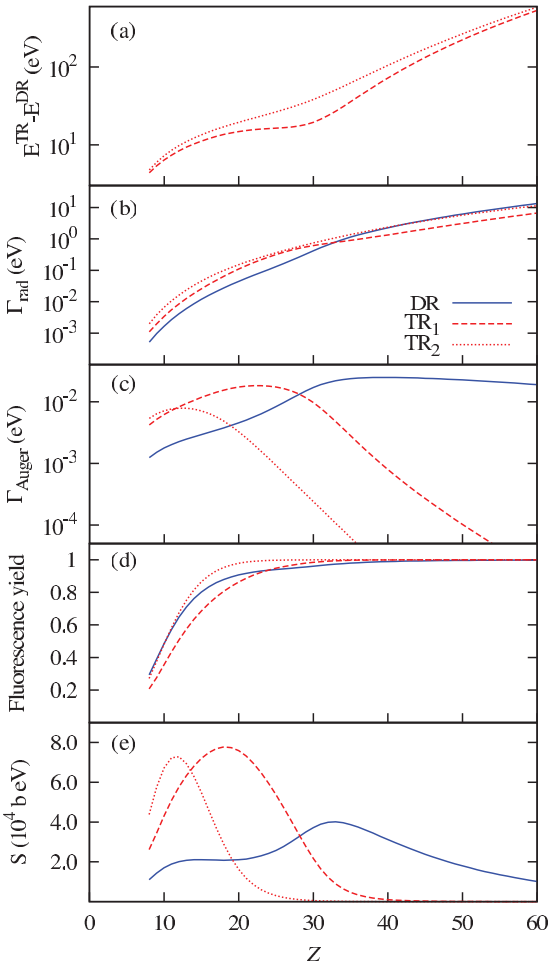

FIG. 10. (Color online) Same as Fig. 9, but for $J = 3/2$ resonances in initially C-like ions. These quantities are given for the case of the $1s2s^22p_{1/2}^2(2p_{3/2}^2)_2$ $J = 3/2$ DR resonance (solid blue line) and the $(1s2s^22p_{1/2})_1 2p_{3/2}^3$ (TR_1, dashed red line) and $(1s2s^22p_{1/2})_0 2p_{3/2}^3$ (TR_2, dotted red line) $J = 3/2$ TR resonances.

parametrization

$$S^{TR} \propto \frac{1}{Z^2} \frac{Z^4 Z^{-2}}{b_1 Z^4 + b_2 Z^0 + b_3 Z^{-2}} = \frac{1}{b_1 Z^4 + b_2 + b_3 Z^{-2}}. \tag{9}$$

At higher atomic numbers, the TR resonance strength decreases as $\propto Z^{-4}$, i.e., significantly faster than the DR strength; therefore, the TR process can hardly be observed in heavier ions.

Independent of that feature, at low Z values, the second-order Auger rate responsible for TR is comparable to or larger than the first-order Auger rate corresponding to DR [see the case with $J = 3/2$ in Fig. 10(c)]. The rate for radiative decay following trielectronic capture may also be larger than the corresponding radiative decay rate for DR [Fig. 10(b)], resulting in a TR resonance stronger than DR. In some cases, e.g., in $J = 5/2$ resonances in initially C-like ions, the three-electron Auger rate may even be weaker than the two-electron Auger rate [see Fig. 9(c)], yet the larger radiative rate overcompensates this and yields a higher strength for TR than for DR.

In the present experiments the total absolute resonance strengths are not accessible directly. However, the calculated ratio of the strength of TR and the corresponding DR process within a single ionic sequence can be compared with the measurements [see the top panel of Fig. 11]. As discussed above, for low Z, the importance of TR increases, and for C-like ions TR dominates over the DR process for $Z < 20$. The sequence for B- and N-like ions shows a similar behavior, but for these charge states TR does not have a dominant influence on the total recombination yield. For Li-like ions, TR contributes very little to the recombination because of the limited number of excitation channels: only one electron is available in the L shell to be excited simultaneously with a K-shell electron.

One can state for the TR/DR strength ratio an excellent agreement between our experimental findings and our calculations. This is not only true for the Z dependence of the strength

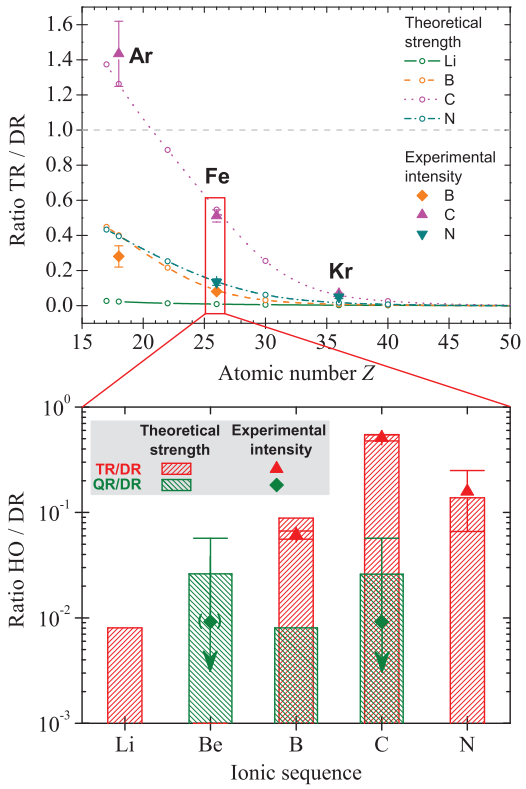

FIG. 11. (Color online) Higher-order TR contributions relative to the corresponding DR resonance strengths as functions of the atomic number Z for Li-like to N-like ionic species. The calculations are compared with the experimental results. (Open circles are calculated *ab initio*, and dashed curves show interpolations; experimental data points show error bars.) For Fe ions, the strength ratios TR/DR and QR/DR for different charge states are given in the bottom graph.

ratio but holds also for the dependence on the ionic sequence. In the bottom panel of Fig. 11 we display for Li- to N-like Fe ions the corresponding strength ratio TR/DR including the ratio QR/DR.

For Fe ions, the nuclear charge Z is low enough to show sizable contributions of higher-order resonances and high enough to ensure a good resolution of the resonance spectrum. The QR/DR strength ratio seems also be confirmed within the experimental uncertainty by the calculations. Although the statistics for QR are insufficient for a precise determination of resonance energies, the spectrum shown in Figs. 6 and 8 shows an obvious indication of QR resonances. Our calculations and the experimental findings agree convincingly well (see the correspondingly marked resonance in Fig. 6). The faint structures seen around an electron energy of 4.980 keV correspond thus to QR in both C- and Be-like Fe ions.

An approximate scaling law for QR may be derived in an analogous manner to that found for TR, using similar considerations for the four-electron Auger rate ($\Gamma^{a,4e} \propto Z^{-4}$):

$$S^{\mathrm{QR}} \propto 1/Z^2 \frac{Z^4 Z^{-4}}{c_1 Z^4 + c_2 Z^0 + c_3 Z^{-2} + c_4 Z^{-4}} = \frac{1}{c_1 Z^6 + c_2 Z^2 + c_3 + c_4 Z^{-2}}. \quad (10)$$

Here, we have taken into account that autoionizing states formed by quadruelectronic capture may decay by two-, three-, or four-electron Auger processes. The QR resonance strength diminishes for high Z even faster than the strength of TR, namely, as $\propto Z^{-6}$. However, its experimental signatures have become measurable, and a systematic study of the interesting isoelectronic sequences as a function of Z could provide better insight into the complex mutual interactions of same-shell electrons, beyond what is possible by studying the single neutrals giving name to those sequences.

V. CONCLUSIONS

Unexpectedly large contributions of higher-order electronic recombination processes have been found for intershell K-L excitation. For these processes, high momenta are exchanged during recombination, and hence, large contributions from higher orders are generally not expected. As shown, the second-order resonant electron recombination process, TR, may even overwhelm the strength of the first-order DR process, as observed in the case of C-like Ar [cf. Fig. 11]. In most cases, the second-order TR process contributes about 10% to the total electronic recombination cross section, and its relative strength decreases with increasing Z. Even the third-order process, QR, was clearly identified, contributing typically a few percent of DR. These findings on the importance of higher-order processes in resonant intershell electronic recombination were made possible by enhanced energy resolution and good experimental statistics, both points being achieved by evaporative axial cooling of the trapped ions.

Beyond the obvious Z trends seen in the resonance energies and caused by the balance between electron correlation and relativistic effects, strikingly apparent higher-order electron-electron correlation effects are found at lower atomic numbers. Here, the strength of higher-order recombination processes can surpass that of the corresponding first-order DR process [14].

Since the intershell K-LL photorecombination process is a far more efficient cooling mechanism in high-temperature plasmas than intrashell processes, due to the much higher energy of the emitted photons, a good knowledge of its energy-dependent cross section is essential. Therefore, hitherto neglected contributions from higher-order effects to electron recombination, especially of the second order (the trielectronic channel), have to be taken into account. Plasma simulations used for modeling fusion devices or astrophysical matter have to include them for improved accuracy. The presence of sizable TR resonances has implications for the opacity and energy transfer inside the radiative zone of stars and for the temperature and ionization equilibrium of those and other astrophysical plasmas. Models not considering these higher-order effects in plasmas containing light-Z species can therefore not describe correctly the status in a plasma. Moreover, for the time-reversed processes of resonant photoionization [40], i.e., the resonant excitation to an autoionizing intermediate state, those higher-order processes may also be of equal importance. Even beyond TR, quadruelectronic recombination has been observed for different ionic species.

Studying photorecombination in all orders of complexity, from DR to TR and QR, could become a fruitful approach for understanding more complex multielectron processes such as

shake-up and shake-off in outer shells, especially for heavier species [41,42]. Arguably, even higher recombination orders involving more than four simultaneous electronic excitations, which are more likely to be expected in recombination of open M-shell ions having many equivalent electrons and vacancies energetically closely spaced, should be investigated to learn about the stepwise buildup of a many-electron wave function. The role of relativistic corrections to the Coulomb electron interaction, i.e., the Breit interaction [37,43], in such higher-order processes is also an unexplored field. With the ion charge as a variable parameter and a constant number of electrons, isoelectronic sequences in highly charged ions are perfectly suited for this type of investigation. Furthermore, such a multielectron behavior may also be manifested in resonant processes occurring due to the presence of neighboring atoms or ions in dense plasmas or molecules [44,45].

ACKNOWLEDGMENT

The work of Z.H. was supported by the Alliance Program of the Helmholtz Association (HA216/EMMI).

[1] H. S. W. Massey and D. R. Bates, Rep. Prog. Phys. **9**, 62 (1942).
[2] A. Burgess, Astrophys. J. **139**, 776 (1964).
[3] D. A. Knapp, R. E. Marrs, M. A. Levine, C. L. Bennett, M. H. Chen, J. R. Henderson, M. B. Schneider, and J. H. Scofield, Phys. Rev. Lett. **62**, 2104 (1989).
[4] D. R. DeWitt, D. Schneider, M. W. Clark, M. H. Chen, and D. Church, Phys. Rev. A **44**, 7185 (1991).
[5] P. Beiersdorfer, T. W. Phillips, K. L. Wong, R. E. Marrs, and D. A. Vogel, Phys. Rev. A **46**, 3812 (1992).
[6] V. V. Flambaum, A. A. Gribakina, G. F. Gribakin, and C. Harabati, Phys. Rev. A **66**, 012713 (2002).
[7] A. J. González Martínez, J. R. Crespo López-Urrutia, J. Braun, G. Brenner, H. Bruhns, A. Lapierre, V. Mironov, R. Soria Orts, H. Tawara, M. Trinczek *et al.*, Phys. Rev. Lett. **94**, 203201 (2005).
[8] Z. Harman, I. I. Tupitsyn, A. N. Artemyev, U. D. Jentschura, C. H. Keitel, J. R. Crespo López-Urrutia, A. J. González Martínez, H. Tawara, and J. Ullrich, Phys. Rev. A **73**, 052711 (2006).
[9] C. Brandau, C. Kozhuharov, Z. Harman, A. Müller, S. Schippers, Y. S. Kozhedub, D. Bernhardt, S. Böhm, J. Jacobi, E. W. Schmidt *et al.*, Phys. Rev. Lett. **100**, 073201 (2008).
[10] A. Müller, Adv. At. Mol. Opt. Phys. **55**, 293 (2008).
[11] S. Schippers, J. Phys. Conf. Ser. **163**, 012001 (2009).
[12] D. A. Knapp, P. Beiersdorfer, M. H. Chen, J. H. Scofield, and D. Schneider, Phys. Rev. Lett. **74**, 54 (1995).
[13] C. Beilmann, O. Postavaru, L. H. Arntzen, R. Ginzel, C. H. Keitel, V. Mäckel, P. H. Mokler, M. C. Simon, H. Tawara, I. I. Tupitsyn *et al.*, Phys. Rev. A **80**, 050702 (2009).
[14] C. Beilmann, P. H. Mokler, S. Bernitt, C. H. Keitel, J. Ullrich, J. R. Crespo López-Urrutia, and Z. Harman, Phys. Rev. Lett. **107**, 143201 (2011).
[15] M. Schnell, G. Gwinner, N. R. Badnell, M. E. Bannister, S. Böhm, J. Colgan, S. Kieslich, S. D. Loch, D. Mitnik, A. Müller *et al.*, Phys. Rev. Lett. **91**, 043001 (2003).
[16] I. Orban, S. D. Loch, S. Böhm, and R. Schuch, Astrophys. J. **721**, 1603 (2010).
[17] S. Schippers, M. Lestinsky, A. Müller, D. W. Savin, E. W. Schmidt, and A. Wolf, Int. Rev. At. Mol. Phys. **1**, 109 (2010).
[18] I. P. Grant, D. F. Mayers, and N. C. Pyper, J. Phys. B **9**, 2777 (1976).
[19] J. R. Crespo López-Urrutia, A. Dorn, R. Moshammer, and J. Ullrich, Phys. Scr. T **80B**, 502 (1999).
[20] S. W. Epp, J. R. Crespo López-Urrutia, G. Brenner, V. Mäckel, P. H. Mokler, R. Treusch, M. Kuhlmann, M. V. Yurkov, J. Feldhaus, J. R. Schneider *et al.*, Phys. Rev. Lett. **98**, 183001 (2007).
[21] K. Widmann, P. Beiersdorfer, V. Decaux, S. R. Elliott, D. Knapp, A. Osterheld, M. Bitter, and A. Smith, Rev. Sci. Instrum. **66**, 761 (1995).
[22] M. Bitter, H. Hsuan, C. Bush, S. Cohen, C. J. Cummings, B. Grek, K. W. Hill, J. Schivell, M. Zarnstorff, P. Beiersdorfer *et al.*, Phys. Rev. Lett. **71**, 1007 (1993).
[23] M. Bitter, M. F. Gu, L. A. Vainshtein, P. Beiersdorfer, G. Bertschinger, O. Marchuk, R. Bell, B. LeBlanc, K. W. Hill, D. Johnson *et al.*, Phys. Rev. Lett. **91**, 265001 (2003).
[24] S. L. Haan and V. L. Jacobs, Phys. Rev. A **40**, 80 (1989).
[25] P. Zimmerer, N. Grün, and W. Scheid, Phys. Lett. A **148**, 457 (1990).
[26] M. Zimmermann, N. Grün, and W. Scheid, J. Phys. B **30**, 5259 (1997).
[27] J. Eichler and W. E. Meyerhof, *Relativistic Atomic Collisions* (Academic, San Diego, CA, 1995).
[28] A. J. González Martínez, J. R. Crespo López-Urrutia, J. Braun, G. Brenner, H. Bruhns, A. Lapierre, V. Mironov, R. Soria Orts, H. Tawara, M. Trinczek *et al.*, Phys. Rev. A **73**, 052710 (2006).
[29] F. A. Parpia, Fischer, and I. P. Grant, Comput. Phys. Commun. **94**, 249 (1996).
[30] S. Zakowicz, Z. Harman, N. Grün, and W. Scheid, Phys. Rev. A **68**, 042711 (2003).
[31] C. Beilmann, P. Amaro, H. Bekker, Z. Harman, J. R. Crespo López-Urrutia, and S. Tashenov, Phys. Scr. T **156**, 014052 (2013).
[32] D. A. Knapp, R. E. Marrs, M. B. Schneider, M. H. Chen, M. A. Levine, and P. Lee, Phys. Rev. A **47**, 2039 (1993).
[33] B. M. Penetrante, J. N. Bardsley, M. A. Levine, D. A. Knapp, and R. E. Marrs, Phys. Rev. A **43**, 4873 (1991).
[34] B. M. Penetrante, J. N. Bardsley, D. DeWitt, M. Clark, and D. Schneider, Phys. Rev. A **43**, 4861 (1991).
[35] C. Beilmann, J. R. Crespo López-Urrutia, P. H. Mokler, and J. Ullrich, J. Instrum. **5**, C09002 (2010).
[36] P. H. Mokler and F. Folkmann, *Structure and Collisions of Ions and Atoms*, Topics in Current Physics Vol. 5 (Springer, Berlin, 1978).
[37] P. Zimmerer, N. Grün, and W. Scheid, J. Phys. B **24**, 2633 (1991).

[38] H. Watanabe, F. J. Currell, H. Kuramoto, S. Ohtani, B. E. O'Rourke, and X. M. Tong, J. Phys. B **35**, 5095 (2002).

[39] A. P. Kavanagh, H. Watanabe, Y. M. Li, B. E. O'Rourke, H. Tobiyama, N. Nakamura, S. McMahon, C. Yamada, S. Ohtani, and F. J. Currell, Phys. Rev. A **81**, 022712 (2010).

[40] M. C. Simon, J. R. Crespo López-Urrutia, C. Beilmann, M. Schwarz, Z. Harman, S. W. Epp, B. L. Schmitt, T. M. Baumann, E. Behar, S. Bernitt *et al.*, Phys. Rev. Lett. **105**, 183001 (2010).

[41] H. Aksela, A. Aksela, and N. Kabachnik, *Resonant and Nonresonant Auger Recombination* (Plenum, New York, 1996), p. 401.

[42] M. Uiberacker, T. Uphues, M. Schultze, A. J. Verhoef, V. Yakovlev, M. F. Kling, J. Rauschenberger, N. M. Kabachnik, H. Schroder, M. Lezius *et al.*, Nature (London) **446**, 627 (2007).

[43] S. Fritzsche, A. Surzhykov, and T. Stöhlker, Phys. Rev. Lett. **103**, 113001 (2009).

[44] C. Müller, A. B. Voitkiv, J. R. Crespo López-Urrutia, and Z. Harman, Phys. Rev. Lett. **104**, 233202 (2010).

[45] A. B. Voitkiv and B. Najjari, Phys. Rev. A **82**, 052708 (2010).